

Magnitude and timing of annual maximum floods: Trends and large-scale climatic associations for the Blacksmith Fork River, Utah

Shaleen Jain and Upmanu Lall

Utah Water Research Laboratory, Utah State University, Logan

Abstract. The magnitude and timing of spring snowmelt floods reflects seasonal snow accumulation and spring temperature patterns. Consequently, interannual variations in regions such as the intermountain West, with snowmelt annual maximum floods, may be related to low-frequency variations in winter/spring large-scale climate variability. Changes in the seasonality of basin precipitation and temperature consequent to slow changes in the baseline climate state (e.g., owing to natural climate variations and/or potential global warming trends) may have significant impacts on such floods. A case study of the Blacksmith Fork River in northern Utah that explores such a hypothesis is presented here. Trends and associations in the magnitude and timing of annual maximum floods are documented, their impact on time-varying estimates of the 100 year flood is assessed, and relationships with known large-scale, quasi-oscillatory patterns of climate variability are explored. Evidence for structured low-frequency variation in flood timing and magnitude and its relation to winter/spring precipitation and temperature and to tropical (El Niño–Southern Oscillation) and extratropical (Pacific Decadal Oscillation) Pacific climate precursors is presented. Mechanisms for these ocean-atmosphere teleconnections to basin precipitation, temperature, and flood potential are discussed.

1. Introduction

Hydrologists have generally considered floods as an outcome of a stationary, independent and identically distributed (i.i.d.) random process [e.g., Kite, 1975; Bobee and Ashkar, 1991]. However, there is growing evidence of trends (which may be related to anthropogenic influences) and long-term variability (related to the natural variability of the climate system) in streamflow records [Cayan and Peterson, 1989; Lins and Michaels, 1994; Lins and Slack, 1999; Baldwin and Lall, 1999] at various timescales. Porporato and Ridolfi [1998] show that weak trends may exert a strong influence on flood exceedance probabilities. The recent increase in extreme floods for the American River in Sacramento, California, provides a key example of such a concern [National Research Council (NRC), 1995, 1999]. For the American River the correspondence in the trends for (1) more extreme spring floods with earlier snowmelt and large rain events and (2) large-scale climate associations has been documented [Roos, 1987; Dettinger and Cayan, 1995; NRC, 1999].

It is our perception that the stationary, i.i.d. approach to flood frequency analysis has prevailed in the hydrologic literature owing to (1) limited records, (2) a focus on at-site, local physical processes, (3) a latent bias associating floods with convective thunderstorms and intense rainfall events, (4) disciplinary boundaries limiting hydrologists' knowledge of climatic processes, (5) the lack of a statistical tool set to analyze and represent extremes and make decisions under nonstationarity, and (6) institutional factors. The i.i.d. assumption has been questioned by considering annual maximum floods to arise from a mixture of causative mechanisms and identifying

these mechanisms in terms of atmospheric circulation types that produced summer floods in Arizona [Hirschboeck, 1987; Webb and Betancourt, 1992]. In the context of interannual to interdecadal climate variability, slowly evolving large-scale climate signals may be useful precursors for the impending basin flood response.

The dynamics of spring snowmelt floods is of particular interest in this context since antecedent soil moisture conditions and the state of the snowpack reflect seasonal evolution and the melt period temperature and rainfall may reflect large-scale climate patterns that can also be diagnosed. Given that relatively long records of monthly climate indices are available, the connection of such seasonal climate variations to floods poses a diagnostic problem that can, perhaps, be related to large-scale, low-frequency climate variations more easily than in environments where daily atmospheric circulation patterns related to intense rainfall and to interstorm event soil moisture conditions need to be diagnosed. Our interest here is in exploring such connections for the Blacksmith Fork River (BFR) in the Great Salt Lake basin in Utah, where prior work [Lall and Mann, 1995; Mann et al., 1995; Moon and Lall, 1996; Rajagopalan and Lall, 1998] has connected the interannual and interdecadal fluctuations of basin hydrologic processes to indices of low-frequency climate variability. Trends in the flood magnitude and timing are identified and related to interannual (El Niño–Southern Oscillation (ENSO)) and interdecadal (Pacific Decadal Oscillation (PDO)) climate indices and to the cold season Pacific Ocean sea surface temperature (SST) and hemispheric atmospheric pressure fields.

2. Interannual and Interdecadal Modes of Climate Variability

Recent decades have seen significant progress in the understanding of the interannual and interdecadal modes of climate

Copyright 2000 by the American Geophysical Union.

Paper number 2000WR900183.
0043-1397/00/2000WR900183\$09.00

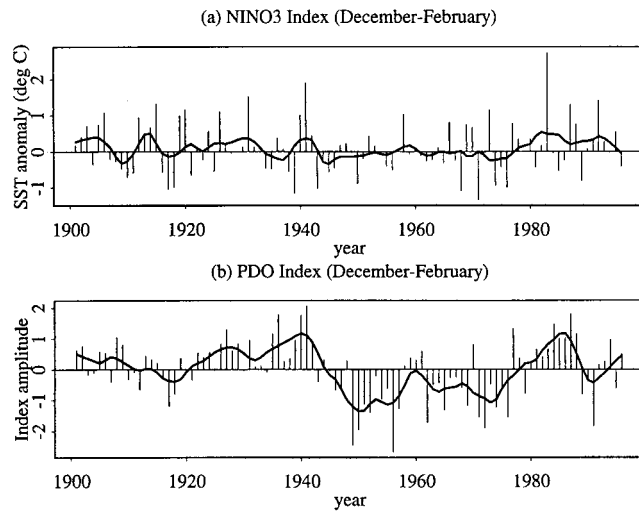


Figure 1. Historical record of the winter season large-scale climate indices. (a) NINO3 and (b) Pacific Decadal Oscillation (PDO) Index. The solid line represents a moving window mean computed using lowess (locally weighted linear regression) [Cleveland and Devlin, 1988] with a ~ 10 year span.

variability and their role as key drivers of long-term hydroclimatic variability at various spatial scales. Dominant interannual modes, such as the tropical ENSO exhibit teleconnections (significant covariations) with seasonal temperatures and precipitation across the globe [Rasmusson and Carpenter, 1982; Ropelewski and Halpert, 1987; Lau and Sheu, 1988; Halpert and Ropelewski, 1992]. ENSO variations occur on 2–7 year time-scales, with origins in the coupled ocean-atmosphere system of the tropical Pacific [Philander, 1990]. During the El Niño (La Niña) phase, anomalously warm (cold) SSTs are observed in the eastern tropical Pacific, accompanied by increased (decreased) convection and cloudiness. Effects of the ENSO are communicated to the extratropics through anomalous upper tropospheric divergence anomalies that affect the Rossby waves (and the large-scale atmospheric circulation). Anomalous circulations, aided by land-ocean contrasts and the internal dynamics of the extratropics, can cause the anomalies to persist for a season or longer. Consequently, the strength and trajectories of the midlatitude storm tracks may undergo significant modulations, causing anomalous temperature and precipitation anomalies over the continents. Indeed, over the North American region the variability in the storm tracks shows close associations with the Pacific teleconnections [Lau, 1988; Trenberth *et al.*, 1998]. ENSO activity and its teleconnections have also undergone significant interdecadal- and century-scale variations as noted by Rajagopalan *et al.* [1997], Trenberth and Hoar [1997], McCabe and Dettinger [1999], Cole and Cook [1998], and Mann *et al.* [2000].

Interdecadal climate fluctuations over the North Pacific covary with the winter surface climate over North America [Mantua *et al.*, 1997]. Further, Mantua *et al.* [1997] found that the principal mode of snowpack variability [Cayan, 1996] over the western United States shows strong associations with the PDO. Gershunov and Barnett [1998] have assessed the joint influence of PDO and ENSO in determining the precipitation and sea level pressure variations over the United States. The mechanistic understanding of the decadal- to century-scale climate variations is an area of current research [e.g., Latif and Barnett,

1994; Nakamura *et al.*, 1997]. There is some debate as to whether the PDO is a phenomenon that is independent of ENSO or part of the same large-scale ocean-atmosphere dynamics. Recent model results suggest a possible physical connection between the northern Pacific decadal variability and the potential modulation of ENSO on decadal scales [Barnett *et al.*, 1999].

Low-frequency modes of large-scale climate are often diagnosed through climate indices. The sea surface temperature anomaly in the so-called “NINO3” region in the eastern equatorial Pacific (5°N – 5°S and 150°W – 90°W) is used as an indicator of ENSO. Figure 1a shows the historical record of the wintertime NINO3 index. The interdecadal signal in the extratropics is represented by the PDO index (Figure 1b), which is the leading principal component of the gridded, monthly SST anomalies in the North Pacific Ocean, poleward of 20°N [Mantua *et al.*, 1997]. We have used these two indices as measures of the low-frequency variability that have potential to modulate the hydrologic response in the western United States.

3. Data Sources and Site Information

The 1914–1996 record for the BFR near Hyrum, Utah (U.S. Geological Survey (USGS) station number 10113500), is listed as being minimally affected by diversions and human influences [Slack *et al.*, 1992]. The drainage area of this gage is 681 km^2 (263 miles^2). The USGS gaging station is located at 1530 m (5021 feet) above the National Geodetic Vertical Datum. This gage was selected because it has one of the more complete, clean, long records in the basin, and the annual maximum flows are well correlated with those for other streams (e.g., Logan River, 0.74 and Weber River, 0.55) in the region, for the common period of record. The drainage basin is largely an undisturbed mountain watershed with national forest, rangeland, and recreation uses. In terms of ENSO influence, the National Oceanic and Atmospheric Administration (NOAA) list this region (see details on the World Wide Web at http://nic.fb4.noaa.gov:80/products/analysis_monitoring/ensostuff/states/UT.html) as one that has only weak correlations with ENSO. However, Gershunov [1998] identifies connections of the ENSO and PDO to early spring snow water equivalent and precipitation and temperature extremes, respectively. Lall and Mann [1995] found the monthly flows of the same gage and regional monthly precipitation, temperature, and streamflow time series to be spectrally coherent with ENSO indicators at the relevant interannual frequencies. They found that signatures of low-frequency variations explain 38% of the total interannual variance of the BFR series. Further, the quasidecadal variations in BFR flows show coherent variations with indices of the large-scale atmospheric circulation [Mann *et al.*, 1995]. Generally, this watershed is at the limit of what is considered to be a region influenced by moisture and heat fluxes during El Niño events and is more influenced by the moisture fluxes and upper jet stream configuration typical of La Niña events that affects the Pacific Northwest with positive winter/spring moisture anomalies. The ENSO response is consequently likely to be nonlinear (dependent on the strength of El Niño events) and asymmetric (more influence during La Niña than El Niño events) with potential North Pacific modulating influences.

The precipitation and temperature data are the 1895–1999 monthly record for the climate division (see details on the World Wide Web at <http://www.ncdc.noaa.gov/onlineprod/>

drought/main.html) for the BFR region. A 1899–1997 gridded monthly record [Trenberth and Paolino, 1980] of Northern Hemisphere sea level pressure (SLP) was also used to investigate the large-scale atmospheric circulation anomalies that may contribute to changes in the flood response. This SLP data set is compiled from a variety of sources; data archive and potential errors in the pre-1945 data are documented on the National Center for Atmospheric Research (NCAR) web site (<http://www.scd.ucar.edu/dss/datasets/ds010.1.html>). The NINO3 and PDO data sets were acquired from the University of Washington (see <http://www.atmos.washington.edu/~mantua/abst.PDO.html>) and the NOAA Climate Prediction Center (see <ftp://ftp.ncep.noaa.gov/pub/cpc/wd52dg/data/indices/sstoi.indices>).

4. Historical Trends in BFR Annual Maximum Floods

The historical record of the BFR annual maximum floods is shown in Figure 2a. The record-breaking flood of May 1917 on the BFR is listed in the chronology of major flood events in the United States [Hoyt and Langbein, 1955]. The 1914–1996 record of annual maximum floods has eight major events that exceeded $28.3 \text{ m}^3/\text{s}$ (7 times the base discharge of $3.9 \text{ m}^3/\text{s}$, over twice the median flood value of $13.3 \text{ m}^3/\text{s}$). The long-term variability of the flood magnitudes shows no statistically significant monotonic trends. However, a spectral analysis using the multitaper method (MTM) [Thomson, 1982; Lall and Mann, 1995] of the flood data reveals statistically significant variance in both the interannual and interdecadal bands (Figure 2b). The quasi-biennial peaks (~ 2.2 years or 0.45 and 0.47 cycles per year) are noted in ENSO indices as well, and the analysis of PDO series shows significant variance in the 16–20 year and the 30 year band (peaks at 18.2 and 31.9 years). ENSO is typically characterized by variability in the 2–7 year range, with MTM indicating peaks at $\sim 2, 3, 5,$ and 7.5 years [Mann and Park, 1994]. The BFR spectrum exhibits peaks at all these frequencies, but only the quasi-biennial and the low-frequency decadal peaks are statistically significant. These frequencies are consistent with the regional and hemispheric climate analyses reported by Lall and Mann [1995] and Mann et al. [1995].

Flood peaks generally occur in late spring for rivers in northern Utah (median flood timing is May 1 for the Blacksmith Fork River). Decadal and longer variations in the timing of annual maximum floods over the twentieth century are highlighted in Figure 2c. From Figure 2d we observe that years in which the annual maximum flood occurs early (before April), the magnitude of the flood is small, reflecting a mild winter snowpack that leads to a “failure” of the flood season. Comparing Figures 2a and 2c, we see that there is some correspondence in the decadal variation in flood timing and magnitude consistent with the relationship between timing and magnitude suggested by Figure 2d.

The 100 year flood is a benchmark of site flood risk for flood insurance and for other flood project analyses. We examined the BFR annual maximum flood data for systematic changes in the 100 year flood. Averaged weather data for a 30 year period are often considered representative of a stable climate [Guttman, 1989]. Thirty years is also the minimum length of record often considered reasonable for reliable 100 year flood estimates. We use a 30 year moving window to compute the mean annual flood, the variance of the annual flood, and the 100 year flood. The lognormal distribution provides a reasonable fit to

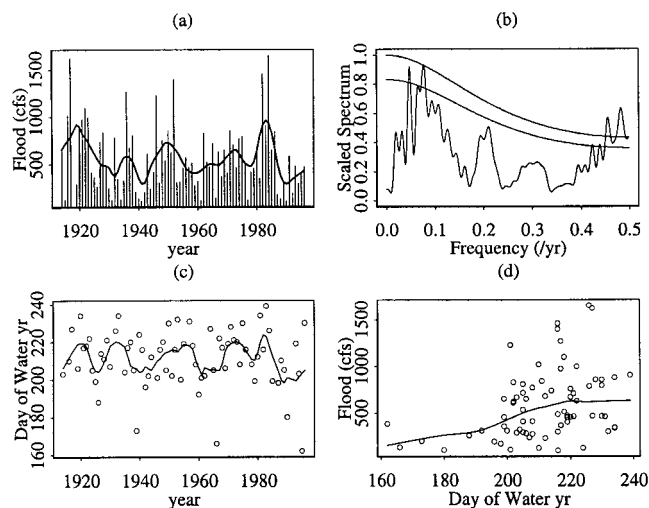


Figure 2. Selected attributes of the Blacksmith Fork River (BFR) annual maximum floods. (a) Historical record. The solid line represents a moving window mean computed using lowess (locally weighted linear regression) [Cleveland and Devlin, 1988] with a 10 year span. This span emphasizes the decadal and longer variability in the flood process. (b) Spectrum computed using the multitaper method [Thomson, 1982] with three 2π tapers. The thin lines correspond to the 90 and 95% confidence levels based on a local red noise significance test [Mann and Lees, 1996]. (c) Variations in the date of occurrence of the spring annual maximum floods for the BFR. The line is a 10 year smooth. (d) Association between the timing and magnitude of annual maximum floods on BFR. The solid line represents a conditional mean computed using lowess with a span equal to two thirds of the data points as neighbors. ($1 \text{ m}^3 \text{ s}^{-1} = 35.31 \text{ cfs}$)

the 82 year flood record for BFR (Figure 3a) based on a chi-square test. The 100 year flood estimates using a lognormal distribution and a 30 year moving window are presented in Figure 3b. The estimates from 30 year windows are plotted near the center of the time interval under consideration. No monotonic trends are evident. However, the estimated 100 year flood varies systematically, decreasing and then increasing over the period of record, with a range that is almost twice the lowest 30 year estimate. There is a relatively sharp decrease in the estimated 100 year flood for 30 year windows centered between 1930 and 1943. It is relatively stable for windows centered between 1955 and 1970, followed by an increase in the subsequent record. Note that if this trend is representative of the regional floods, shorter records in the region may indicate a dramatic recent upward trend that some may consider attributing to anthropogenic factors. Moreover, as with the American River floods [NRC, 1999], it will appear that the level of flood protection in the recent period is less than a 100 years if projects were sized using a 100 year flood estimated from a “low” flood period. Thus the dynamic risk represented by the systematically changing 100 year flood estimate over representative 30 year windows needs further investigation.

Comparing Figure 3b with Figure 2a, it is not altogether obvious that the trends in the annual maximum flood should translate into the trends observed for the estimated 100 year flood. It is useful to diagnose changes in the moving window estimates of 100 year flood through similar changes in the moments of the annual flood process. Recall that the 100 year

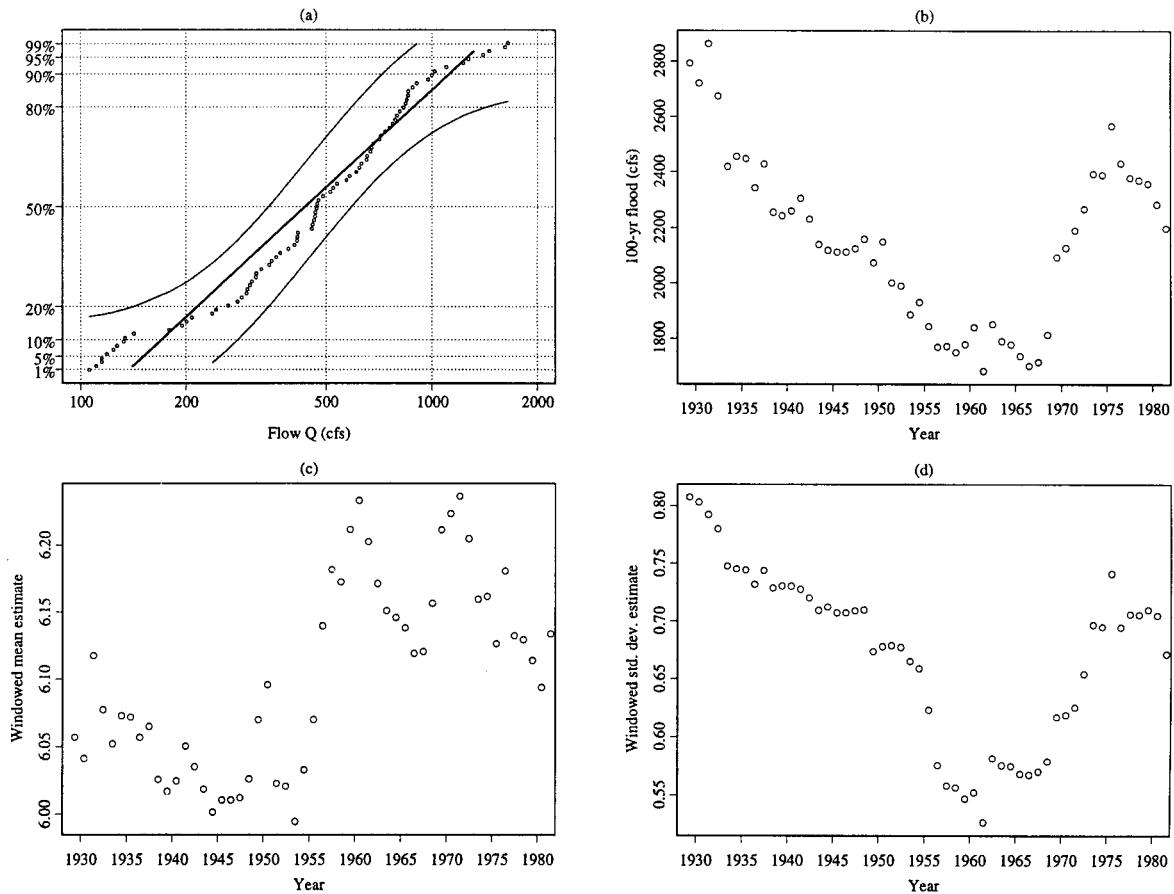


Figure 3. (a) A quantile plot of the BFR flood flows and the fitted lognormal distribution, with 90% confidence intervals, (b) estimates of the 100 year flood event based on the 30 year windowed estimates using a lognormal distribution, (c) estimated mean (log (annual flood)) using a 30 year moving window, and (d) estimated variance (log (annual flood)) using a 30 year moving window. Note that the first window spans from 1914 to 1943, and the last window spans from 1965 to 1996. Plotting positions are at the center of the 30 year time window.

flood is estimated here as the sum of the mean annual flood and the standard deviation of the annual maximum flood times a frequency factor for the lognormal distribution. The moving window trends in the mean and standard deviation of the log (annual flood) are shown in Figures 3c and 3d, respectively. The standard deviation of the annual flood process is marked by a decreasing trend for windows centered between 1933 and 1970 and an increasing trend thereafter. The decrease in the estimated 100 year flood in the early part of the record corresponds to this trend since the mean annual flood is relatively stable over that period. Interestingly, the mean annual flood appears to be marked by two regimes separated by a rather sharp transition centered around 1952–1962. The recent increase in the estimated 100 year flood corresponds to the recent increasing trend in the standard deviation and the increased mean flood level. The middle period of record with a relatively constant estimate of the 100 year flood corresponds to offsetting upward and downward trends in the mean and standard deviation.

5. Climate Composites for High and Low BFR Floods

Winter snow storms as well as melt period advective heat fluxes and moisture are brought to the northern Utah/BFR

region by a series of migratory winter storms with typical life cycles of 1–4 days. These storms typically track the principal midlatitude jet stream patterns and principal SLP anomalies (such as the ones associated with the quasi-permanent Aleutian low). Further, climate in this arid Great Basin region is controlled by the combined influence of large-scale climate anomalies and the local troughs that modulate precipitation and temperatures [Cayan and Peterson, 1989]. In this context, Robertson and Ghil [1999] discuss the role of large-scale weather regimes that modulate the winter precipitation and temperature over the western United States. Local precipitation and temperature modulation by (1) displaced storm tracks and (2) the warm and cold air advection are seen as principal carriers of the anomalous large-scale climate signal that has associations with ENSO and extratropical SST anomalies. Further, Cayan and Redmond [1999] find significant influence exerted by the extreme phases of ENSO, on the relative frequency of heavy precipitation and associated streamflow. However, the BFR region is on the boundary of the strongly ENSO influenced regions of the western United States and the cold season snowpack dynamics is potentially influenced by both PDO and ENSO. Therefore it is of interest to investigate how changes in the winter/spring precipitation and temperature over the BFR region influence the ensuing flood response

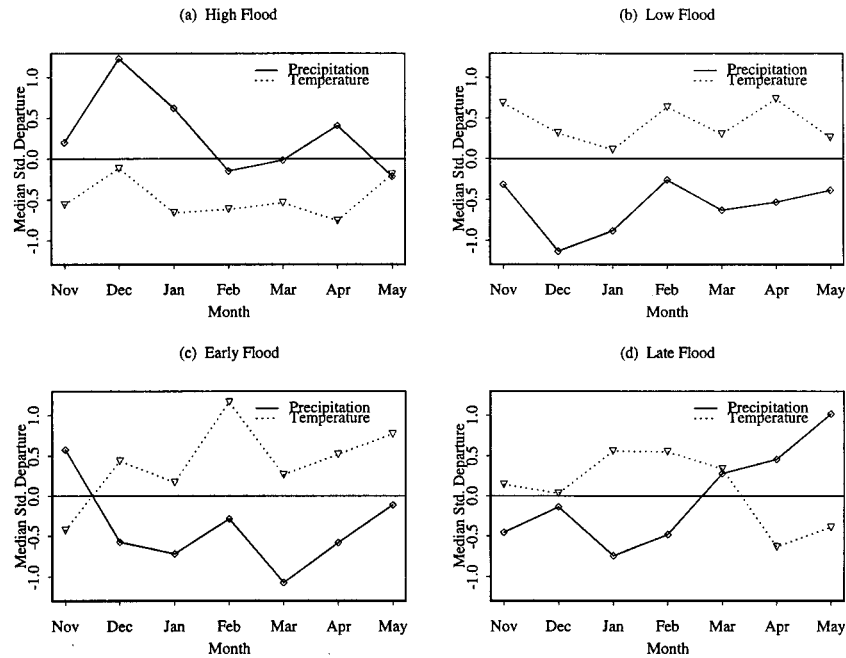


Figure 4. Median standardized departures for precipitation and temperature. (a) High flood, (b) low flood, (c) early flood, and (d) late flood. The median standardized departures are computed as median of the November–May precipitation and temperature anomalies 10 events in each category.

and, in turn, are themselves modulated by Pacific Ocean and hemispheric atmospheric flow patterns.

Average standardized anomalies of monthly temperature and precipitation in the BFR region corresponding to the years with the 10 largest and 10 smallest floods are shown in Figures 4a and 4b. Corresponding anomalies for years with the 10 earliest and the 10 latest floods are shown in Figures 4c and 4d. For the low flood years the median anomaly pattern is a persistently warm November–May period combined with a significantly below normal precipitation (Figure 4b). The high floods result in years when the combined influence of high rainfall in relatively cold winters help develop and sustain a snowpack until the spring, when it melts, causing high floods (Figure 4a). Early floods correspond to a very warm and dry January–May period, and as seen in Figure 2d, they correspond to low floods. The late annual maximum flood events appear to correspond to cooler, wetter conditions in the typical snowmelt season (Figure 4d), following a warmer, drier winter.

Associations between extreme BFR floods and large-scale climate were explored by examining the composite winter atmospheric and ocean circulation patterns for the 10 highest and 10 lowest flood years. The average SLP anomalies from January, February, and March (JFM) season SLP conditions (computed as departures from the long-term mean conditions that are illustrated as contours in Figure 5c) for high and low flood years are shown in Figures 5a and 5b, respectively. The high (low) flood years are associated with a weakened (deepened) Aleutian low. Aleutian low anomalies are part of the larger-scale Pacific North American pattern, which is, in turn, significantly modulated by the ENSO phase. For BFR the high floods result in years with a weaker Aleutian low (frequently associated with the La Niña phase). During the La Niña years the storms are steered northward toward the Aleutians and the Gulf of Alaska; this may reinforce the westerly and northwesterly storm tracks that bring moisture to the Pacific Northwest

and the Great Basin region. Further, the extratropical low-frequency variability (in part tracked by the PDO) also contributes to maintenance and variability of the winter circulation patterns over the western United States. *Chen and van den Dool* [1999] note that the La Niña winters (often associated with high floods in BFR) exhibit a stronger low-frequency component (e.g., associated with persistent blocking) in the extratropics, suggesting the importance of both tropical and extratropical low-frequency variability in determining the winter season variability. In contrast, during the El Niño winters, high-frequency transients dominate and play a vital role in reinforcing the subtropical jet that is steered to the southwest United States. For the low floods the anomaly center is shifted northwest, off of the Aleutian islands (Figure 5b). Anomaly projections for high and low years are shown in Figure 5c with the horizontal component of the vector representing the high flood years and the vertical component representing the low flood years. The source areas of variability are centered over the North Pacific Ocean. Further, given the alignment of vectors away from the 45° line, the asymmetry in forcing response is also evident. The asymmetry reflects the nonlinear nature of large-scale climate response and the year-to-year changes in the anomaly patterns. The overall nature of SLP pattern departures shows a clear response in the anomaly fields where high and low flood composites are subtracted (Figure 5d). Perhaps, the most evident feature is the clarity of anomalous circulation fields.

The oceans are arguably the carriers of the long-term climate signal. They provide slowly changing boundary conditions for the atmosphere that lend interannual “memory” to atmospheric processes. Consequently, an examination of the composite January–March (JFM) SST fields for the 10 highest and 10 lowest flood years is useful in understanding the SLP anomalies discussed above. The Pacific SST anomalies corresponding to the previous SLP analysis are shown in Figure 6. Note

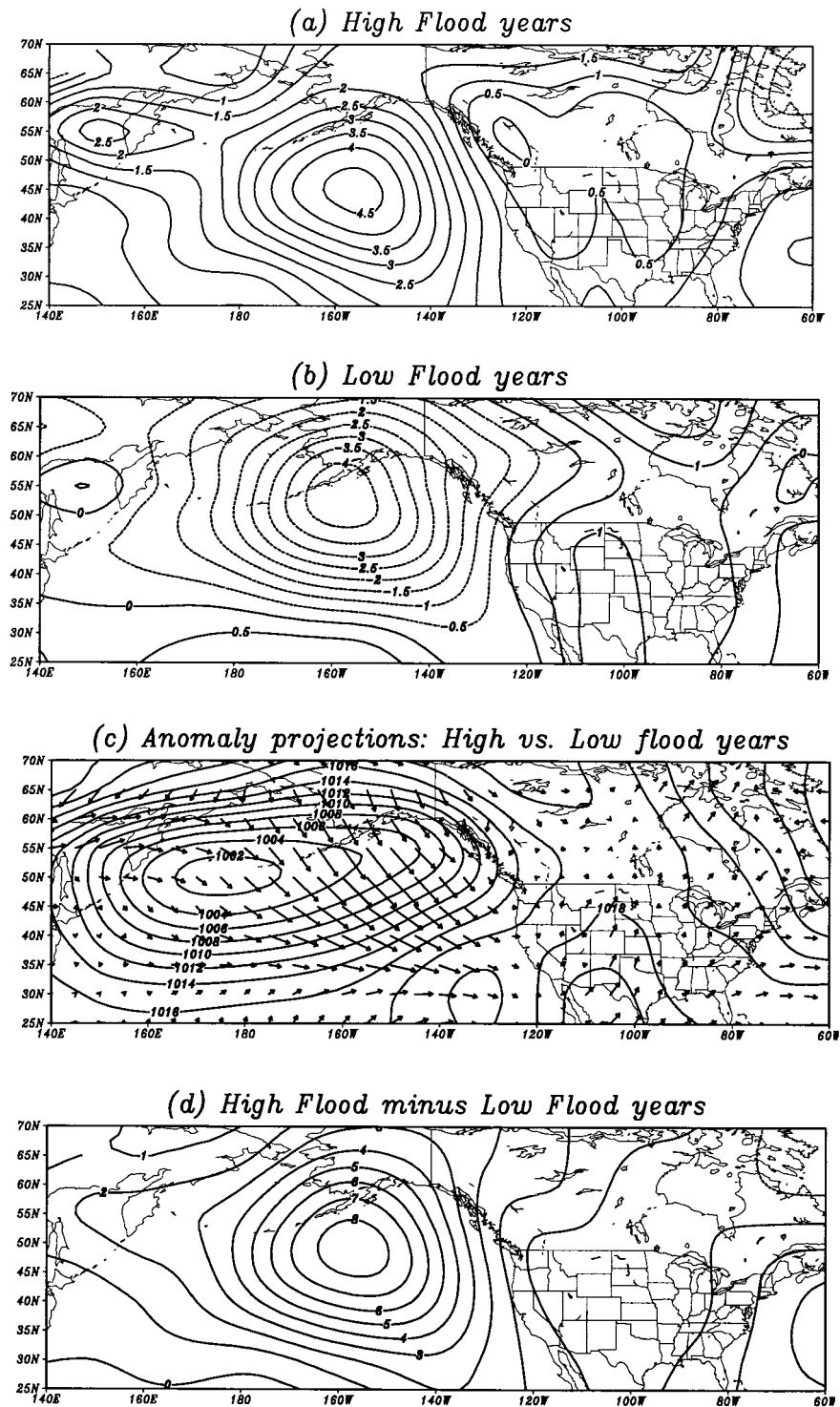


Figure 5. Large-scale winter (January–March (JFM)) sea level pressure fields over the Pacific North American region. (a) Composite anomaly fields for 10 high flood years for BFR. (b) Composite anomaly fields for 10 low flood years for BFR. (c) Anomaly projections for the high and low flood years. The horizontal component of the anomaly vector corresponds to the high floods, and the vertical component corresponds to the low flood. It is evident that the source regions of anomaly fields are over the North Pacific and the Aleutian Islands. The asymmetry in response suggests that the anomaly fields may not be all linear. The contours represent the 1961–1990 JFM climatology for the SLP. (d) Sea level pressure anomaly fields obtained by differencing Figures 5a and 5b. These emphasize the linear component of the overall anomaly response associated with the high and low floods over BFR. Note that anomalies are computed as departures from a 1961–1990 SLP climatology.

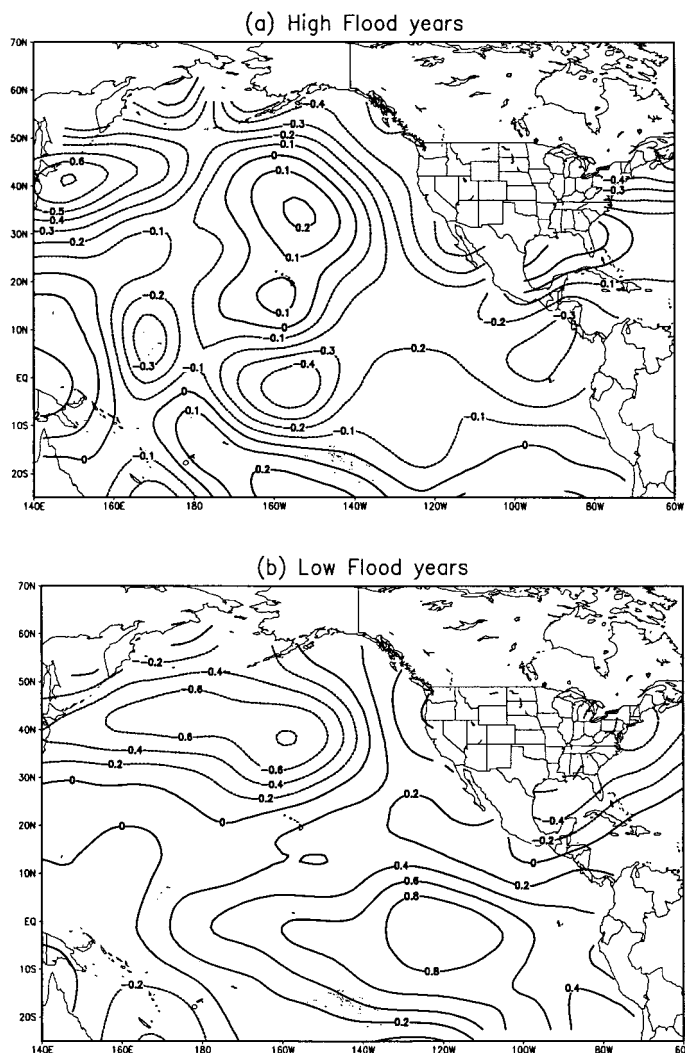


Figure 6. Winter (JFM) sea surface temperature (SST) anomaly fields over the Pacific Ocean. (a) North Pacific and tropical Pacific SST composite anomalies corresponding to high flood years. (b) North Pacific and tropical Pacific SST composite anomalies corresponding to low flood years. Note that anomalies are computed as departures from a 1961–1990 SST climatology.

that the latitude range in Figure 6 is expanded over that in Figure 5. The stronger Aleutian low in low flood years seems to correspond to cooler temperatures in the central North Pacific and warmer temperatures off the northwest U.S. coast. Warmer eastern tropical Pacific conditions that are typically associated with El Niño events are also evident in the low flood composite. The weaker Aleutian low in high flood years corresponds to a more zonal flow structure corresponding to a warmer central North Pacific and cooler coastal North Pacific. The tropical Pacific SST structure for high flood years is not as readily interpreted as an ENSO phase. A closer examination of the two largest flood events, in 1917 and 1984, is interesting. January through March 1917 is marked by a strong La Niña event [Allan *et al.*, 1996, p. 251] in a negative PDO phase, while January through March 1984 is marked by a dissipating El Niño event in a strongly positive PDO phase. Thus there is a suggestion that high BFR floods may occur in either phase of ENSO, as modulated by the state of the extratropical Pacific.

The analysis provided in this section suggests that organized large-scale winter SST and SLP patterns in the tropical and extratropical Pacific Ocean region may influence extreme flood

occurrence for the BFR. The patterns of climatic variability identified appear to relate to the ENSO and PDO modes of interannual and interdecadal variability documented in the literature [Mantua *et al.*, 1997].

6. Climate Indices and BFR Floods, Precipitation P , and Temperature T

In this section the “transfer functions” of flood season basin precipitation, temperature, and floods to the NINO3 and PDO indices are empirically explored. The hope is that as the understanding and predictability of ENSO and PDO variations improve, knowledge of the teleconnections of basin hydroclimate to the ENSO and PDO indices could be used to diagnose and predict flood risk. Our empirical investigation of the BFR floods is based on a joint analysis of the historical data for floods, P , T , and climate indices (PDO and NINO3). Since the basin flood response is largely snowmelt driven, we chose cold season precipitation (November–March), winter temperature (January–March), spring temperature (March–May), spring precipitation (March–May), NINO3 (January–March), and

Table 1. Correlations Between the Key Observables That Determine the Annual Maximum Flood Response for Blacksmith Fork River, Utah^a

	Log (Flood)	DOWY	NINO3	PDO	<i>T</i> (JFM)	<i>P</i> (NDJFM)	<i>T</i> (MAM)	<i>P</i> (MAM)
log (Flood)	1	0.37 ^b	-0.34 ^b	-0.32 ^b	-0.28 ^b	0.72 ^b	-0.45 ^b	0.38 ^b
DOWY		1	-0.12	0.02	-0.25 ^b	0.26 ^b	-0.44 ^b	0.36 ^b
NINO3			1	0.41 ^b	0.11	-0.23 ^b	0.05	-0.02
PDO				1	0.17	-0.34 ^b	0.13	-0.05
<i>T</i> (JFM)					1	-0.18	0.55 ^b	0.13
<i>P</i> (NDJFM)						1	-0.25 ^b	0.35 ^b
<i>T</i> (MAM)							1	-0.37 ^b
<i>P</i> (MAM)								1

^aDOWY, Day of Water Year; *T*, temperature; *P*, precipitation.

^bCorrelations significant at the 5% level.

PDO (January–March) as key indicators of the seasonally averaged hydroclimatic state.

Pairwise correlations between selected state variables are presented first to assess the linear response of basin variables to the two climate indices and also the relationship between seasonal precipitation, temperature, and flood peak and timing. Partial correlations of flood statistics on PDO and NINO3 given one or the other indicator are also presented. Kernel regression methods are next used to identify the nature of the joint, nonlinear dependence of flood magnitudes on PDO and NINO3. A “treed regression” approach is used to classify NINO3 and PDO combinations that lead to particular BFR flood responses. An investigation of the relative frequency of occurrence of each of these climate index classes over the period of record is finally used to provide insights on how the time variations in the climatic precursors of BFR floods relate to the variations in flood risk.

6.1. Correlation Analyses

Correlations among the key basin-scale observables and the NINO3 and PDO indices are summarized in Table 1. Analysis of cross correlations across the various observables allows an assessment of the extent to which the low-frequency precursors exert a linear. The translation of the anomalous low-frequency signal may be carried forth by the basin-scale observables, through a modulation of snowpack dynamics and/or the direct runoff in spring.

The logarithm of annual peak flood is positively correlated with the day of water year (DOWY), consistent with the relation seen in Figure 2d that showed smaller floods coming earlier. Likewise, the timing of the peak flood is positively correlated with the winter and spring precipitation and negatively correlated with the temperature in these seasons. The annual peak flood is negatively correlated with both the PDO and the NINO3 index, suggesting that at least in a linear response sense, one should expect larger floods in La Niña years with the PDO in a negative phase. This is the case for 4 of the 10 largest floods. However, the DOWY, is not significantly correlated with either of the climate indices. The correlations discussed thus far are confirmed by the pairwise correlations between the remaining variables. The only additional observation of interest is the persistence in the winter and spring precipitation and temperature, as evidenced by the positive correlation in the same variable across the two seasons. We also observe that the NINO3 and the PDO indices are significantly correlated with each other. Consequently, it is necessary to diagnose whether both are needed to explain the BFR flood response. The partial correlation of the log (flood)

with NINO3, given PDO, is -0.24 , and the partial correlation of the log (flood) with PDO given NINO3 is -0.21 . These are smaller than the raw correlations, as expected. However, they are still significant at the 5% level, suggesting that both indices are needed to diagnose the BFR variations. The multiple R^2 for the linear regression of the log (annual flood) on NINO3 and PDO is only 0.15.

6.2. Nonlinear Associations of the BFR Floods and the Climate Indices

Recognizing that even in a linear sense, both the NINO3 and the PDO are useful precursors of the BFR floods, we investigated the potential nonlinear relationship between the flood series and the two indices using nonparametric kernel regression. The conditional mean (Figure 7) and the conditional variance (Figure 8) of the BFR floods given the winter PDO and the winter NINO3 were evaluated using the procedure described in Appendix 1. The highest floods seem to correspond to a condition when both the PDO and the NINO3 are at their negative extremes. However, moderately large floods also tend to occur corresponding to a positive NINO3 (i.e., El Niño condition) in combination with a positive PDO and to a strongly negative PDO in combination with an El Niño condition. Thus selected combinations of the extreme phases of the tropical and the extratropical SST oscillation indices appear to lead to higher flood potential in the BFR. The log (flood) variance is reduced for the extreme positive and negative phases of the PDO, with a maximum when the PDO is inactive, for negative NINO3 (La Niña conditions). The variance in-

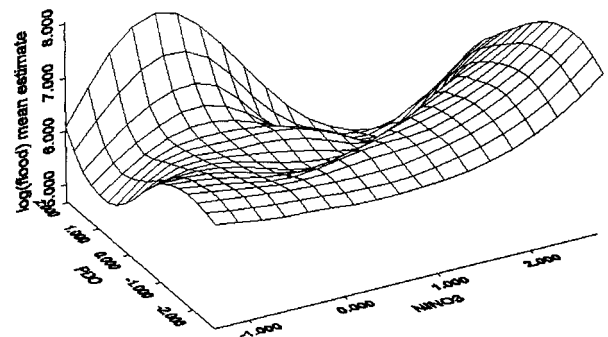


Figure 7. Estimates of log (flood) based on the nonparametric smoothed estimates. The joint influence of the NINO3 and PDO evinces nonlinear associations. Climate indices are based on the December–February averages.

creases with NINO3 when PDO is inactive and increases with PDO when NINO3 is inactive.

A treed regression algorithm [Alexander and Grimshaw, 1996] was used to partition the predictor space of PDO and NINO3 into distinct partitions formed by recursive univariate splits along each predictor axis. Each partition has a separate linear regression equation for the log (flood) as a function of the two climate indices, which is fit over the domain of the partition. The minimum number of observations to keep in a partition can be specified. The procedure is similar to multivariate adaptive regression splines [Friedman, 1991], except that continuity of the regression surface across partitions is not preserved, the regressions are linear rather than cubic, and more detailed diagnostics of the regression in each partition are presented. Given that the partitions are adaptively chosen, this is also a nonparametric regression approach similar to the kernel regressions presented earlier. The primary difference is that the regression function is not assumed to be continuous or smooth, the boundary effects that plague kernel regression near the ends of the data are likely ameliorated, and the resulting classification of the predictor space is interpretable in terms of distinct predictor regimes that correspond to different responses of the floods. We present both analyses here partly to ensure that the conclusions are not affected by the details of the approach used and because they provide somewhat different information and interpretability. The partitions determined by the treed regression approach are illustrated in Figure 9. The overall coefficient of determination R^2 for the fitted treed regression model is 0.4. The partitioned domains in Figure 9 correspond to the relative phase of the PDO and ENSO. The key observations (see Figure 9) are (1) partition I, corresponding to a positive PDO phase with La Niña to transition El Niño conditions, accounts for 5 of the 10 largest floods and 1 of the 10 lowest floods; (2) partition II, corresponding to positive PDO and El Niño conditions, corresponds to 5 of the 10 smallest floods and none of the 10 highest floods; (3) partition III, corresponding to El Niño conditions and the negative and neutral phases of the PDO, corresponds to 2 of the 10 smallest floods and 1 of the 10 largest; (4) partition IV, corresponding to negative PDO and La Niña to transition El Niño conditions, accounts for 4 of the 10 largest floods and 1 of the 10 smallest floods; and (5) partition V, corresponding to neutral PDO conditions and La Niña to transition El Niño conditions, corresponds to 1 of the 10 smallest and none of the 10 largest floods. The interaction between the extreme phases of the PDO and the NINO3 in determining flood potential is thus evident.

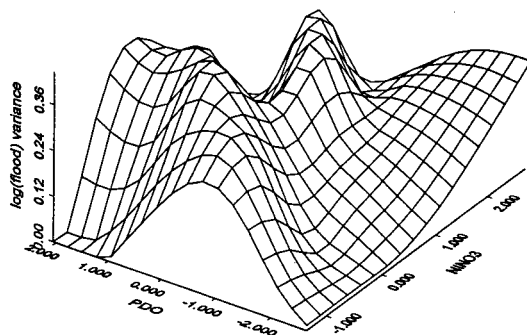


Figure 8. Estimates of log (flood) variance based on the non-parametric smoothed estimates. The joint influence of the NINO3 and PDO evinces nonlinear associations.

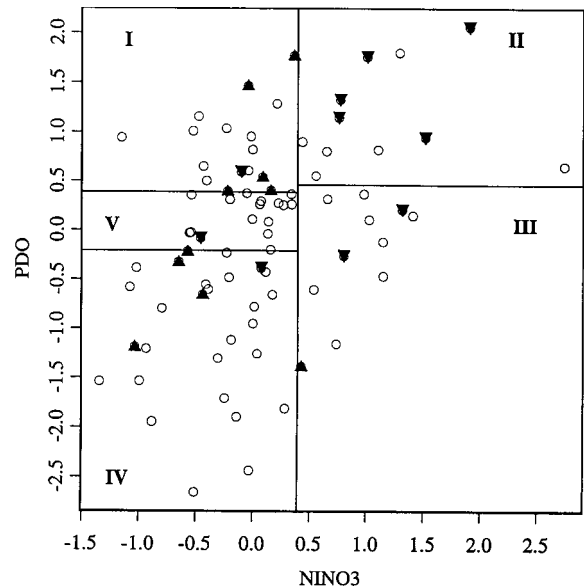


Figure 9. Treed regression model for the BFR floods based jointly on the states of NINO3 and PDO ($R^2 = 0.4$). Partitions of the predictor space are determined by the treed regression approach. The partitions delineate the NINO3-PDO space into regions with distinct regression relationships. Solid triangles represent the 10 highest (upward pointing triangles) and the ten lowest (downward pointing triangles) floods in the BFR record.

7. Summary

The investigations presented here were motivated by observations of long-term and interannual/decadal trends in annual maximum flood series in a region where “conventional wisdom” assumes that ENSO teleconnections are weak. We identified precipitation and temperature regimes that correspond to the changing flood timing and magnitudes over the period of record and then proceeded with an empirical investigation of the relation of the flood magnitudes to large-scale climate modes. The two large-scale climate indices, NINO3 and PDO, were found to explain 40% of the variance of the annual maximum flood series through a nonlinear regression with an identification of the dominant classes of PDO and NINO3 combinations that lead to high and low annual floods. We terminated our investigations at the classification stage and did not test a predictive annual flood-forecasting model in split sample mode.

Recognizing that ENSO variations have a characteristic variability in the 2–7 year frequency band and that the PDO has a characteristic period in excess of 16 years, this work provides an example of how slowly varying climate states that may have regime like structure may affect finite sample flood statistics that lead to apparent nonstationarities in the flood record. Such examples are clearly useful for retrospective diagnoses. However, the longer-term interest is in developing parsimonious models for at-site or regional flood probabilities that can be conditioned on simple climate indicators (whose variability can be represented through an appropriate time series model). Such models could provide estimates of conditional flood risk and also help develop a better understanding of the behavior of the tails of flood distributions from finite samples, where the causative flood processes are persistent or slowly varying re-

gime-like states that can be identified using systematic or proxy data. Research in this direction is in progress.

The work presented here also has implications for the development of regional flood frequency analysis relationships. There are often dramatic differences in the period of record associated with each of the stations used in a regional regression or other regional flood estimation approach. Where the flood-generating process is assumed to be independent and identically distributed in time, techniques such as generalized least squares that address the changing sample estimation variance as a function of sample size may be adequate for estimating improved regional regression equations. However, where slowly varying climate regimes systematically affect regional flood potential, these differences may translate into significant biases in the regional flood equations, as well as a weakening of the potential relationship. We are currently analyzing regional floods in this context, with the goal of developing improved regional flood frequency estimation procedures that can account for the potentially strong spatial correlation of floods that result from slowly varying large-scale climate variations that can, in turn, be modeled.

Appendix 1: Nonparametric Smoothing Estimators for the Flood Mean and Variance

The variability of the flood mean and variance as a function of the ENSO and PDO state was assessed through the nonparametric kernel density estimation (KDE). The resulting estimates provide a robust weighted averaging of the flood data. We use a multivariate generalization of the Nadaraya-Watson kernel regression estimator [Härdle, 1990]. Define

$$\mathbf{u}_i = \frac{(\mathbf{x} - \mathbf{x}_i)^T \sum_{\mathbf{x}}^{-1} (\mathbf{x} - \mathbf{x}_i)}{h^2} \quad (\text{A1})$$

$$K(\mathbf{u}_i) = \frac{1}{2\pi} e^{-\mathbf{u}_i^2/2}, \quad (\text{A2})$$

where \mathbf{u}_i is a Mahalanobis distance between the vectors \mathbf{x} and \mathbf{x}_i , $\sum_{\mathbf{x}}$ is the covariance matrix of \mathbf{x} estimated from the full historical sample, h is a scalar bandwidth, and $K(\cdot)$ is a Gaussian kernel or weight function.

The bandwidth h used for the bivariate \mathbf{x} data was taken to be the optimal bandwidth for a bivariate Gaussian distribution [Silverman, 1986, p. 87].

$$h_{\text{opt}} = 0.96n^{-1/6}. \quad (\text{A3})$$

The kernel regression is used here largely as an exploratory plotting tool. Consequently, the reference bandwidth approach was considered adequate.

The conditional expectation and variance of the log annual maximum flood values y given the NINO3 and PDO values \mathbf{x} can be expressed as

$$E[y|\mathbf{x}] = \sum_i y_i \frac{K(\mathbf{u}_i)}{\sum K(\mathbf{u}_i)} \quad (\text{A4})$$

$$\text{var}[y|\mathbf{x}] = \sum_i (y_i - E[y|\mathbf{x}])^2 \frac{K(\mathbf{u}_i)}{\sum K(\mathbf{u}_i)}, \quad (\text{A5})$$

where E is the expected value.

Acknowledgments. This work was supported in part by the NSF grant EAR 9720134. The authors wish to thank Scott D. Grimshaw for providing the Treed regression codes. Thanks are also due to Michael Mann for the spectral analysis codes.

References

- Alexander, W. P., and S. D. Grimshaw, Treed regression, *J. Comput. Graphical Stat.*, 5, 156–175, 1996.
- Allan, R., J. Lindsay, and D. Parker, *El Niño Southern Oscillation and Climate Variability*, 405 pp., CSIRO, Melbourne, Australia, 1996.
- Baldwin, C. K., and U. Lall, Seasonality of streamflow: The upper Mississippi River, *Water Resour. Res.*, 35, 1143–1154, 1999.
- Barnett, T. P., D. W. Pierce, M. Latif, and D. Dommengat, Interdecadal interactions between the tropics and midlatitudes in the Pacific basin, *Geophys. Res. Lett.*, 26(5), 615–618, 1999.
- Bobee, B., and F. Ashkar, *The Gamma Family and Derived Distributions Applied in Hydrology*, 203 pp., Water Resour., Littleton, Colo., 1991.
- Cayan, D. R., Interannual climate variability and snowpack in the western United States, *J. Clim.*, 9, 928–948, 1996.
- Cayan, D. R., and D. H. Peterson, The influence of North Pacific atmospheric circulation on streamflow in the West, in *Aspects of Climate Variability in the Pacific and the Western Americas*, *Geophys. Monogr. Ser.*, vol. 55, edited by D. H. Peterson, pp. 375–397, AGU, Washington, D. C., 1989.
- Cayan, D. R., and K. T. Redmond, ENSO and hydrologic extremes in the western United States, *J. Clim.*, 12, 2881–2893, 1999.
- Chen, W. Y., and H. M. van den Dool, Significant change of extratropical natural variability and potential predictability associated with the El Niño/Southern Oscillation, *Tellus, Ser. A*, 51, 790–802, 1999.
- Cleveland, W. S., and S. J. Devlin, Locally-weighted regression: An approach to regression analysis by local fitting, *JASA J. Am. Stat. Assoc.*, 83, 596–610, 1988.
- Cole, J. E., and E. R. Cook, The changing relationship between ENSO variability and moisture balance in the continental United States, *Geophys. Res. Lett.*, 25, 4529–4532, 1998.
- Dettinger, M. D., and D. R. Cayan, Large-scale atmospheric forcing of recent trends toward early snowmelt runoff in California, *J. Clim.*, 8, 606–623, 1995.
- Friedman, J. M., Multivariate adaptive regression splines, *Ann. Stat.*, 19, 1–141, 1991.
- Gershunov, A., Interdecadal modulation of ENSO teleconnections, *Bull. Am. Meteorol. Soc.*, 79, 2715–2725, 1998.
- Gershunov, A., and T. Barnett, ENSO influence on intraseasonal extreme rainfall and temperature frequencies in the contiguous United States: Observations and model results, *J. Clim.*, 11, 1575–1586, 1998.
- Guttman, N. B., Statistical descriptors of climate, *Bull. Am. Meteorol. Soc.*, 70, 602–607, 1989.
- Halpert, M. S., and C. F. Ropelewski, Temperature patterns associated with the Southern Oscillation, *J. Clim.*, 5, 577–593, 1992.
- Härdle, W., *Applied Nonparametric Regression*, 333 pp., Cambridge Univ. Press, New York, 1990.
- Hirschboeck, K., Hydroclimatically-defined mixed distributions in partial duration flood series, in *Hydrologic Frequency Modeling*, edited by V. P. Singh, pp. 199–212, D. Reidel, Norwell, Mass., 1987.
- Hoyt, W. G., and W. B. Langbein, *Floods*, 469 pp., Princeton Univ. Press, Princeton, N. J., 1955.
- Kite, G. W., *Frequency and Risk Analysis in Hydrology*, 224 pp., Water Resour., Littleton, Colo., 1975.
- Lall, U., and M. E. Mann, The Great Salt Lake: A barometer for interannual climatic variability, *Water Resour. Res.*, 31(10), 2503–2515, 1995.
- Latif, M., and T. P. Barnett, Causes of decadal climate variability over the North Pacific and North America, *Science*, 266, 634–637, 1994.
- Lau, K.-M., and P. J. Sheu, Annual cycle, quasi-biennial oscillation, and Southern Oscillation in global precipitation, *J. Geophys. Res.*, 93, 10,975–10,988, 1988.
- Lau, N.-C., Variability of the observed midlatitude storm tracks in relations to low-frequency changes in the circulation pattern, *J. Atmos. Sci.*, 45, 2718–2743, 1988.
- Lins, H. F., and P. J. Michaels, Increasing U.S. streamflow linked to greenhouse forcing, *Eos Trans. AGU*, 75(25), 281, 284–285, 1994.
- Lins, H. F., and J. R. Slack, Streamflow trends in the United States, *Geophys. Res. Lett.*, 26, 227–230, 1999.

- Mann, M. E., and J. J. Park, Global-scale models of surface temperature variability on interannual to century timescales, *J. Geophys. Res.*, *99*, 25,819–25,828, 1994.
- Mann, M. E., and J. Lees, Robust estimation of background noise and signal detection in climatic time series, *Clim. Change*, *33*, 409–445, 1996.
- Mann, M. E., U. Lall, and B. Saltzman, Decadal-to-centennial-scale climate variability: Insights into the rise and fall of the Great Salt Lake, *Geophys. Res. Lett.*, *22*, 937–940, 1995.
- Mann, M. E., R. S. Bradley, and M. K. Hughes, Long-term variability in the El Niño Southern Oscillation and associated teleconnections, *El Niño and the Southern Oscillation: Multiscale Variability and its Impacts on Natural Ecosystems and Society*, edited by H. F. Diaz and V. Markgraf, pp. 322–372, Cambridge Univ. Press, New York, 2000.
- Mantua, N. J., S. T. Hare, Y. Zhang, J. M. Wallace, and R. C. Francis, A Pacific interdecadal climate oscillation with impacts on salmon production, *Bull. Am. Meteorol. Soc.*, *78*, 1069–1079, 1997.
- McCabe, G. J., and M. D. Dettinger, Decadal variations in the strength of the ENSO teleconnections with precipitation in the western United States, *Int. J. Clim.*, *19*, 1399–1410, 1999.
- Moon, Y.-I., and U. Lall, Atmospheric flow indices and interannual Great Salt Lake variability, *J. Hydrol. Eng.*, *1*(2), 55–62, 1996.
- Nakamura, H., G. Lin, and T. Yamagata, Decadal climate variability in the North Pacific during the recent decades, *Bull. Am. Meteorol. Soc.*, *98*, 2215–2225, 1997.
- National Research Council (NRC), *Flood Risk Management and the American River Basin: An Evaluation*, 235 pp., Natl. Acad. Press, Washington, D. C., 1995.
- National Research Council (NRC), *Improving American River Flood Frequency Analyses*, 120 pp., Natl. Acad. Press, Washington, D. C., 1999.
- Philander, S. G. H., *El Niño, La Niña, and the Southern Oscillation*, 293 pp., Academic, San Diego, Calif., 1990.
- Porporato, A., and L. Ridolfi, Influence of weak trends on exceedance probability, *Stochastic Hydrol. Hydraul.*, *12*, 1–14, 1998.
- Rajagopalan, B., and U. Lall, Low-frequency variability in western U.S. precipitation, *J. Hydrol.*, *210*, 51–67, 1998.
- Rajagopalan, B., U. Lall, and M. Cane, Anomalous ENSO occurrences: An alternate view, *J. Clim.*, *10*, 2351–2357, 1997.
- Rasmusson, E. M., and T. H. Carpenter, Variations in tropical sea surface temperature and surface wind fields associated with the Southern Oscillation/El Niño, *Mon. Weather Rev.*, *110*, 354–384, 1982.
- Robertson, A. W., and M. Ghil, Large-scale weather regimes and local climate over the western United States, *J. Clim.*, *12*, 1796–1813, 1999.
- Ropelewski, C. F., and M. S. Halpert, Global and regional scale precipitation patterns associated with the El Niño/Southern Oscillation, *Mon. Weather Rev.*, *115*, 1606–1626, 1987.
- Roos, M., Possible changes in the California snowmelt patterns, paper presented at the Fourth Pacific Climate (PACLIM) Workshop, U.S. Geol. Surv., Pacific Grove, Calif., 1987.
- Silverman, B. W., *Density Estimation for Statistics and Data Analysis*, 175 pp., Chapman and Hall, New York, 1986.
- Slack, J. R., J. M. Landwehr, and A. Lumb, A U.S. Geological Survey streamflow data set for the United States for the study of climate variations, 1874–1988, *U.S. Geol. Surv. Open File Rep.*, *92-129*, 200 pp., 1992.
- Thomson, D. J., Spectrum estimation and harmonic analysis, *Proc. IEEE*, *70*, 1055–1096, 1982.
- Trenberth, K. E., and T. J. Hoar, El Niño and climate change, *Geophys. Res. Lett.*, *24*, 3057–3060, 1997.
- Trenberth, K. E., and D. A. Paolino, The Northern Hemisphere sea-level pressure data set: Trends, errors, and discontinuities, *Mon. Weather Rev.*, *108*, 855–872, 1980.
- Trenberth, K. E., G. W. Branstator, D. Karoly, A. Kumar, N.-C. Lau, and C. Ropelewski, Progress during TOGA in understanding and modeling global teleconnections associated with tropical sea surface temperatures, *J. Geophys. Res.*, *103*, 14,291–14,324, 1998.
- Webb, R. H., and J. L. Betancourt, Climate variability and flood frequency of the Santa Cruz River, Pima County, Arizona, *U.S. Geol. Surv. Water Supply Pap.* *2379*, 40 pp., 1992.

S. Jain and U. Lall, Utah Water Research Laboratory, Utah State University, UMC 82, Logan, UT 84322-8200. (sl8gn@cc.usu.edu; ulall@cc.usu.edu)

(Received December 15, 1999; revised May 30, 2000; accepted May 31, 2000.)

